An Inverse Heat Transfer Approach for Evaluating Contact Interface Temperatures in Sliding Contacts

I. Srinivasula Reddy[1], *Sai* Neeraja.V[2], *Vikas* M.[3] , and, *Kishore Kumar Reddy.P*[4*]

[1] Associate Professor, Department of Civil Engineering, K.S.R.M. College of Engineering (Autonomous), Kadapa, Andhra Pradesh-516003, India
[2] Associate Professor, Dept of Civil Engineering, Chaitanya Bharathi Institute of Technology (A), Proddutur-516360, Andhra Pradesh, India.
[3] Assistant Professor, Dept of Civil Engineering, RV College of Engineering(A),Mysuru Road, Bengaluru-560059, Karnataka, India.
[4] Associate Professor, Department of Civil Engineering, Malla Reddy Engineering and Management Sciences (A), Medchal, Telangana-501401, India

Abstract. This research centers on the formulation and evaluation of a simplified inverse thermal analysis framework employing numerical techniques based on discretized elements. Experiments were carried out using Stainless Steel 304 (SS304) material to evaluate the effectiveness of the proposed inverse heat transfer technique. This study aims to evaluate the heat produced by friction at the interface of metallic surfaces under dry sliding conditions. Temperature data were collected at 3 mm and 7 mm from the interface using a pin-on-disk setup. The model integrates FEM with Beck's algorithm for heat flux estimation. To validate the model predictions, transient thermal analysis was performed using ANSYS Workbench.

1 Introduction

Inverse thermal analysis techniques are frequently applied to determine temperature distributions in areas where direct measurement is not possible, such as during welding or casting operations (Repaci, 1991). These models are essential for evaluating interfacial heat transfer coefficients and contact temperatures in applications like friction stir welding, brake systems, and resistance spot welding. Beck et al. (1985) pioneered methodologies for estimating unknown heat sources using remote temperature data, a foundation for later works. Several researchers have built on this, employing analytical (Fernandes et al., 2015),

*Corresponding author: pkkrnitc@gmail.com

finite element (Raghavendra et al., 2019), and finite difference (Sun et al., 2011 and Chen et al., 2014) approaches. Material-specific studies, such as by Aweda and Adeyemi (2009), highlighted the effect of processing conditions on heat transfer coefficients. Recent advancements include machine learning integration (Zhang et al., 2023; Wang et al., 2023) and real-time monitoring techniques (Su et al., 2024), improving the speed and accuracy of inverse solutions. In this study, frictional heat generated during sliding contact of SS304 components was estimated using an inverse thermal conduction framework utilizing the FEM blended with Beck's methodology. Since direct measurement at the interface is impractical, temperatures were recorded away from the contact zone and used to infer interface conditions.

2 2. Materials and methodology

2.1 Materials

SS304 was chosen for this study due to its thermo-physical properties, with supplier-provided data listed in Table 1. Both pin and disk specimens were made from the same material. The pin was 30 mm long with a square cross-section measuring 6 mm on each side, and featured a 3 mm radius cylindrical tip. Figure 1 provides a visual depiction of the pin, including both a photograph and a schematic. Two perpendicular faces were drilled 3 mm deep using a 1.5 mm bit, positioned at distances of 3 mm (Point A) and 7 mm (Point B) from the interface where contact occurs.

Table 1. Thermal and physical properties of SS304 alloy.

Material	Thermal conductivity ($W\ m^{-1}\ °C^{-1}$)	Specific heat ($J\ kg^{-1}\ °C^{-1}$)	Density ($kg\ m^{-3}$)
SS304 alloy	16.2	500	8000

2.2 Experimental setup and procedure

Dry sliding tests used a pin-on-disk configuration with a cylindrical pin and flat surface, both composed of the same material. Test parameters, including load and speed, are listed in Table 2. Frictional heat was generated at the contact interface, but due to limitations in direct measurement, to monitor the temperature, thermocouples of type K were embedded at two distinct depths—near 3 and 7 mm—from the contact interface within the central region of the pin. Data were sampled at 5 Hz with 0.0001 °C accuracy. Results are shown in Fig. 2.

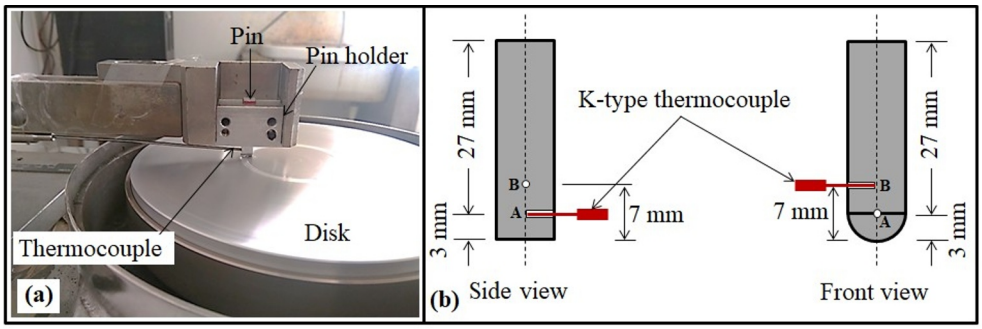

Fig. 1. (a) Pin-on-disk setup during testing. (b) Schematic showing thermocouple positions for temperature measurement in the pin specimen.

Table 2. Dry Sliding Test Experimental Conditions.

Material	Normal load (kg)	Sliding speed (m/s)
SS304	2	1

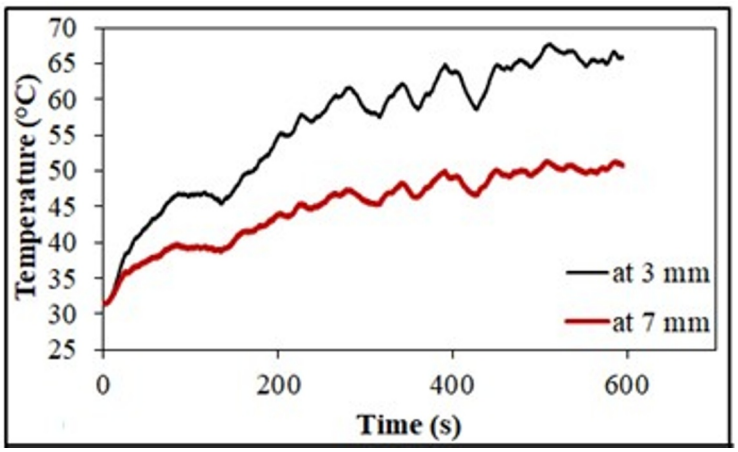

Fig. 2. Heat Profiles at Specified Distances from the Contact Zone in SS304 Sliding Under Dry Conditions.

2.3 Methodology

To estimate the temperature at the contact interface, readings were taken at positions 3 mm and 7 mm away. FEM was used to construct a 1D model of conductive heat transfer, and Beck's technique was applied in an inverse framework to estimate the distribution of temperature and heat flux. The model was validated in ANSYS Workbench using the estimated heat flux and measured temperature at 7 mm.

2.4 Numerical formulation of inverse heat transfer using the finite element method

To support a one-dimensional conductive heat transfer model, temperature data were collected at the mid-plane of the pin (designated as plane 'abcd' in Fig. 3). An assessment of heat transfer was also conducted along this plane, assuming primarily one-dimensional conduction and negligible pin length reduction due to wear. To reduce convective heat loss, measurement points were placed near the contact interface, and the model considers pure conduction. One-dimensional heat conduction is governed by the following equation:

$$\frac{\partial}{\partial x}\left(k\frac{\partial \mathrm{T}}{\partial x}\right)=\rho c\frac{\partial \mathrm{T}}{\partial t} \quad \text{at } 0 < x < \mathrm{L} \text{ and } t = 0; \qquad (1)$$

In this equation, x denotes the distance from the contact interface, k represents the thermal conductivity, ρ is the material's density, c stands for specific heat capacity, T is the temperature, t is

time, and L refers to the pin length (7 mm). The study assumes the pin's initial temperature is uniform and equal to the ambient temperature along its entire length.

Preliminary boundary conditions:

T(x, 0) = Tmea(x = 3 mm, 0 s); (2a)

Heat flux, q(0, 0) = 0; (2b)

Applied Boundary conditions:

T(x = 7 mm, t) = Tmea(x = 7 mm, t); at t > 0; (2c)

q(x = 0 mm, t) = q(t); at t > 0; (2d)

At time 'n', the temperature at two nodes of the element is given by:

$$\left[\frac{\rho c l}{6}\begin{bmatrix}2 & 1\\ 1 & 2\end{bmatrix}+\frac{(\Delta t)k}{l}\begin{bmatrix}1 & -1\\ -1 & 1\end{bmatrix}\right]\begin{Bmatrix}T_i^n\\ T_{i+1}^n\end{Bmatrix}=\frac{\rho c l}{6}\begin{bmatrix}2 & 1\\ 1 & 2\end{bmatrix}\begin{Bmatrix}T_i^{n-1}\\ T_{i+1}^{n-1}\end{Bmatrix}+(\Delta t)\begin{Bmatrix}q_i^n\\ q_{i+1}^n\end{Bmatrix} \quad (3)$$

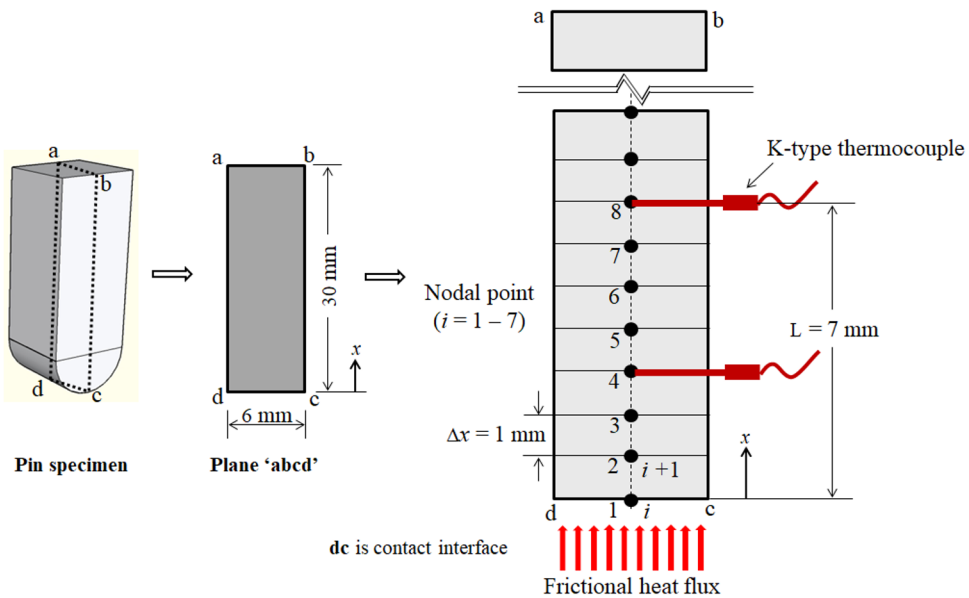

Fig. 3. Discretized Pin Specimen with Applied Boundary Conditions.

The thermal flow at the interface between the bodies is essential for computing the temperature in Equation (3), although it is not available at the outset. This is addressed by assuming a heat flux value, then iteratively correcting it based on measured temperatures at selected locations. A non-linear estimation technique was introduced by Beck et al. (1985) using the least squares technique to relate internal body temperature to surface heat flux. In this study, to estimate heat flux, a one dimensional FEM model was coupled with Beck's technique. An initial heat flux value of 1 was assumed for t > 0 and held constant for u=4 time steps. Temperatures for the subsequent time steps were predicted using this assumed heat flux, then refined by adjusting the flux by a small fraction, εq. Equation (4) was used to calculate the influence of flux variation on nodal temperatures, and the corrected heat flux

was derived from Equation (5). This process was repeated iteratively at each time step until the convergence criterion in Equation (7) was met.

$$\phi_i^{n+j-1} = \frac{T_{est(a)i}^{n+j-1}\Big|_{q+\varepsilon q} - T_{est(a)i}^{n+j-1}\Big|_{q}}{\varepsilon q}; j = 1, 2, \ldots u \tag{4}$$

$$dq^n = \frac{\sum_{i=1}^{m}\sum_{j=1}^{u}\left(\left(T_{mea}^{n+j-1}\Big|_i - T_{est}^{n+j-1}\Big|_i\right)\phi_i^{n+j-1}\right)}{\sum_{i=1}^{m}\sum_{j=1}^{u}\left(\phi_i^{n+j-1}\right)^2}; i = 4,\ j = 1, 2, \ldots u \tag{5}$$

$$q_{cor}^n = q^n + dq^n \tag{6}$$

$$\frac{dq^n}{q^n} \le \varepsilon; \varepsilon = 0.0001 \tag{7}$$

In the model, T_{est} is the estimated temperature, T_{mea} is the measured temperature, q_{cor} is the corrected heat flux, and Δq represents the change in heat flux. The model starts with initial conditions from Equations (2a) and (2b). Accurate heat flux prediction depends on assuming an initial flux lower than the actual value, so at each time step, $q=1\ W/m^2$ is used. With this assumption, the temperature distribution along the 7 mm pin length is computed using Equation (3), under boundary conditions where $T(7,t)=T_{mea}(7,t)$ and $q_n=q_{n+1}=\cdots=q_{n+j+1}$. To correct the assumed heat flux, the estimated and measured temperatures at the 3 mm location (node 4 in Fig. 3) are compared according to Equation (5). The corrected heat flux q_{cor} is then used for the next iteration, repeating until the required accuracy, as defined by Equation (7), is achieved. The inverse heat transfer model, including heat flux and temperature distribution for all time steps, was implemented in MATLAB.

3 Results and discussion

3.1 Temperature Field and Heat Flux Estimated via Inverse Analysis

The sliding of two metallic surfaces against one another induces frictional forces, resulting in localized stress concentrations, plastic deformation, and the generation of heat. Sliding of SS304 alloy at 1 m/s under a 2 kg normal load led to a time-dependent increase in both heat flux and contact temperature. The heat flux predicted at the contact interface is illustrated in Figure 4. The initial rise in heat flux during the first 300 seconds is due to the increasing coefficient of friction, while stabilization reflects steady-state friction. The temperature distribution along the pin's length, estimated at various nodal points, is shown in Figure 5. Understanding the temperature at the contact surface is vital for analyzing frictional and thermal effects at the interface.

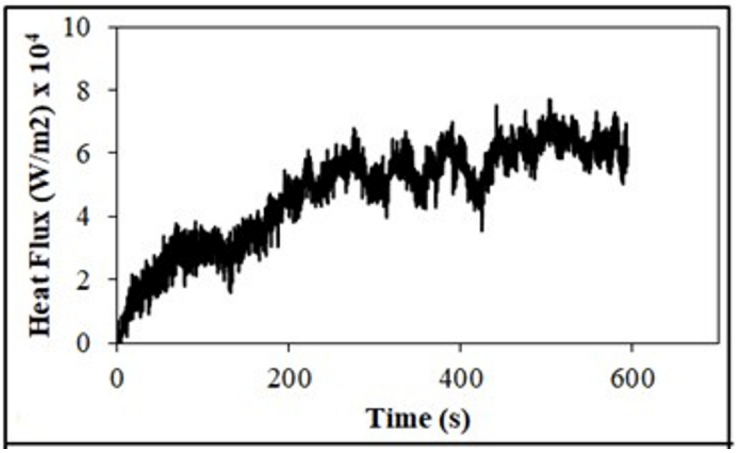

Fig. 4. Evaluated Heat Flux at the Interface in SS304 Sliding Contact.

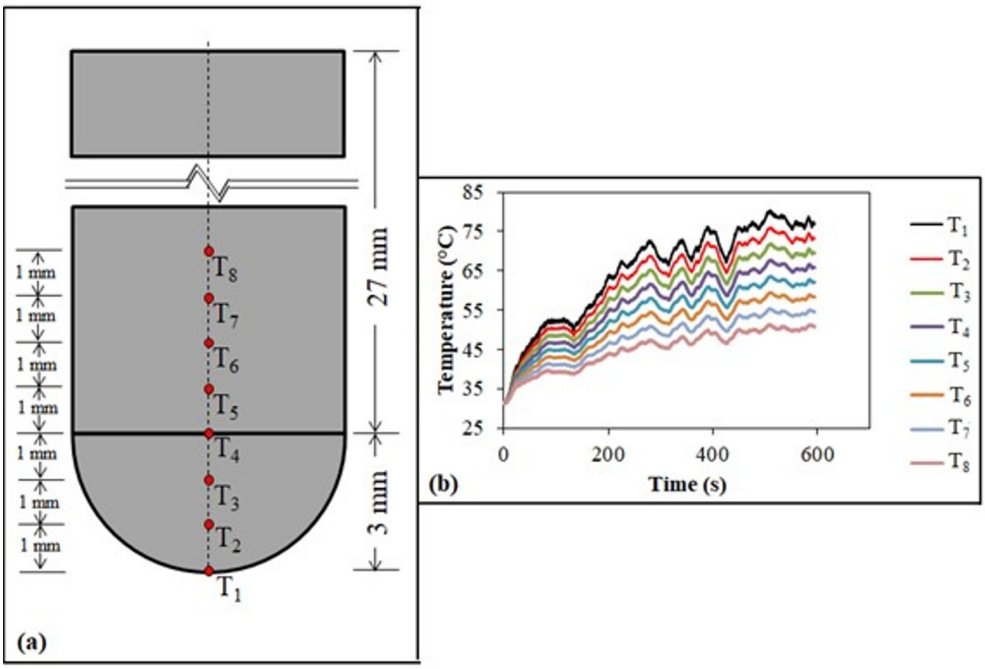

Fig. 5. (a) Pin Specimen Nodal Positions and (b) Calculated Nodal Temperatures in SS304 Alloy.

3.2 Assessment of the Inverse Modeling Accuracy

The inverse model's accuracy was confirmed through comparison with the heat flux data illustrated in Figure 4. ANSYS Workbench was employed to analyze a 7 mm portion of the pin located near the contact interface, comparing simulation results with the model. For the finite element analysis, a PLANE77 element type with 1 mm element size was used.

PLANE77 is a two-dimensional, eight-node thermal element with a single temperature degree of freedom per node. A transient thermal analysis was conducted with the estimated heat flux applied at the contact surface, the measured temperature at the 7 mm location assigned to side 'ab', and the remaining boundaries ('ad' and 'bc') treated as adiabatic. The temperature distributions in the SS304 alloy pins at a specific time, modeled in ANSYS, are shown in Figure 6. The temperature values at each node, derived from the ANSYS simulation and illustrated in Figure 3, were evaluated in comparison with the inverse model predictions. The temperature differences at each node between the two models are plotted in Figure 7. For SS304 alloy, the maximum temperature difference of about 0.4°C was observed during the first few seconds of sliding at the T1 location, with a mean error of 0.03°C across all time steps. For Al 6061-T6 alloy, the mean difference was around 0.006°C. The temperature at the 3 mm location predicted by the ANSYS model was compared with experimental measurements for both alloys. The temperature differences for SS304 are shown in Figure 7. A mean error of 0.05°C was observed when comparing ANSYS results to experimental data for SS304, confirming the accuracy and reliability of the inverse heat transfer model.

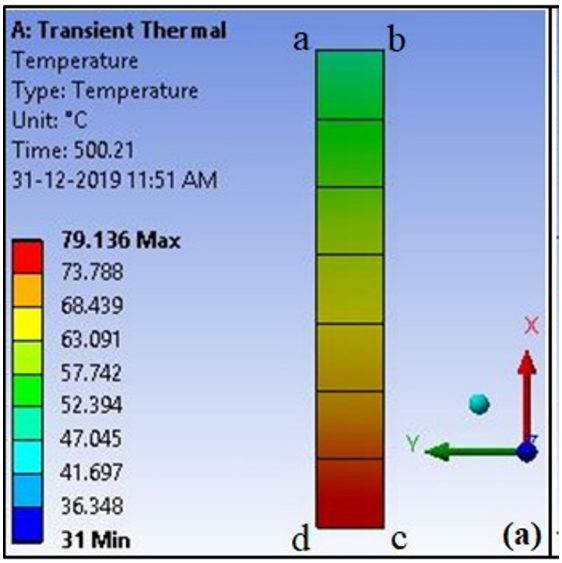

Fig. 6. Temperature Profile in SS304 Alloy Pin at 500.2 s.

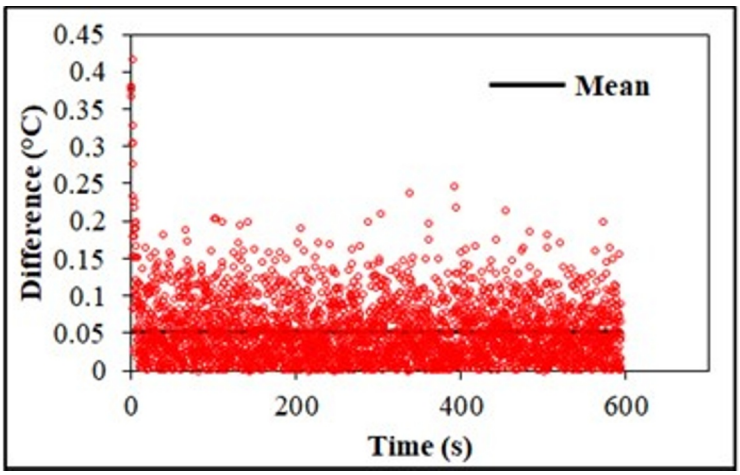

Fig. 7. Analysis of Temperature Differences at 3 mm Location in SS304 Alloy: Simulation and Experimental Data.

4 Conclusions

In this investigation, temperatures were recorded at 3 and 7 mm from the contact interface using K-type thermocouples. SS304 material is selected to assess the robustness of the suggested inverse heat transfer approach. The results demonstrate that the developed model is applicable across a range of materials, particularly in scenarios where convective heat losses are minimal and can be reasonably neglected. Based on insights from existing literature, the proposed inverse model holds potential as an effective alternative method for estimating thermal transfer coefficients during metal casting operations, as well as for determining weld spot temperatures in various welding applications.

References

1. J. O. Aweda, M. B. Adeyemi, Experimental determination of heat transfer coefficients during squeeze casting of aluminium. *J. Mater. Process. Technol.* 209, 1477–1483 (2009).
2. J. V. Beck, B. Blackwell, C. R. St. Clair Jr., *Inverse heat conduction. Ill-posed problems.* John Wiley & Sons, Inc., A Wiley-Interscience Publication (1985).
3. L. Chen, Y. Wang, L. Peng, P. Fu, H. Jiang, Study on the interfacial heat transfer coefficient between AZ91D magnesium alloy and silica sand. *Exp. Therm. Fluid Sci.* 54, 196–203 (2014).
4. A. P. Fernandes, M. B. dos Santos, G. Guimarães, An analytical transfer function method to solve inverse heat conduction problems. *Appl. Math. Model.* 39, 6897–6914 (2015).
5. C. R. Raghavendra, S. Basavarajappa, I. Sogalad, Analysis of temperature field in dry sliding wear test on pin-on-disc. *Heat Mass Transf.* 55, 1545–1552 (2019).
6. A. Repaci, A nonlinear inverse heat transfer problem. *Comput. Math. Appl.* 21, 139–143 (1991).

7. J. Su, H. Zhou, Y. Wu, X. Zhu, Heat source modeling of dissimilar Al/Cu friction stir welding using real-time torque monitoring. *Int. J. Adv. Manuf. Technol.* (2024).
8. Z. Sun, H. Hu, X. Niu, Determination of heat transfer coefficients by extrapolation and numerical inverse methods in squeeze casting of magnesium alloy AM60. *J. Mater. Process. Technol.* 211, 1432–1440 (2011).
9. X. Wang, Y. Liu, H. Zhou, Pipeline fluid temperature recognition based on inverse heat conduction problem using ALO-SSA algorithm. *J. Therm. Anal. Calorim.* (2023).
10. L. Zhang, Y. Zeng, T. Wu, Rapid online solution of inverse heat transfer problems using artificial neural network-based extended Kalman smoothing. *arXiv preprint* arXiv:2304.00021 (2023).
11. Y. Zhang, X. Yang, X. Wei, G. Ma, Y. Liu, Interfacial Heat Transfer Coefficient Variation During Solidification of Circular Steel Castings in Sand Molds. *Int. J. Metalcast.* 17, 117–130 (2023).